Writable spin wave nanochannels in a ferromagnetic thin film mediated by artificial spin ice

Jianhua Li[1,2,3], Wen-Bing Xu[1,2], Wen-Cheng Yue[1,2], Zixiong Yuan[1,2], Tan Gao[1,2], Ting-Ting Wang[1,2], Zhi-Li Xiao[4,5], Yang-Yang Lyu[2], Chong Li[1,2], Chenguang Wang[1,2], Fusheng Ma[6,*], Sining Dong[1,2], Ying Dong[7], Huabing Wang[2,8], Peiheng Wu[2,8], Wai-Kwong Kwok[4] and Yong-Lei Wang[1,2,8*]

[1] *School of Electronic Science and Engineering, Nanjing University, Nanjing, 210023, China*

[2] *Research Institute of Superconductor Electronics, Nanjing University, Nanjing, 210023, China*

[3] *School of Physics and Electronic Electrical Engineering, Huaiyin Normal University, Huaian, 223300, China*

[4] *Materials Science Division, Argonne National Laboratory, Argonne, IL 60439, USA*

[5] *Department of Physics, Northern Illinois University, DeKalb, IL 60115, USA*

[6] *School of Physics and Technology, Nanjing Normal University, Nanjing 210046, China*

[7] *Research Center for Quantum Sensing, Zhejiang Lab, Hangzhou, Zhejiang, 311121, China*

[8] *Purple Mountain Laboratories, Nanjing, China*

* Correspondence to: phymafs@njnu.edu.cn; yongleiwang@nju.edu.cn

Abstract

Magnonics, which employs spin-waves to transmit and process information, is a promising venue for low-power data processing. One of the major challenges is the local control of the spin-wave propagation path. Here, we introduce the concept of writable magnonics by taking advantage of the highly flexible reconfigurability and rewritability of artificial spin ice systems. Using micromagnetic simulations, we show that globally switchable spin-wave propagation and the locally writable spin-wave nanochannels can be realized in a ferromagnetic thin film underlying an artificial pinwheel spin ice. The rewritable magnonics enabled by reconfigurable spin wave nanochannels provides a new setting to design programmable magnonic circuits and logic devices for ultra-low power applications.

1. The challenge to Moore's law due to the physical limitations of electronic devices, has propelled magnonics and/or spintronics as promising venues to transmit and process information with high performance[1-10]. The current research in magnonics is to pave a new way for post-Moore information and communications technology[1-10]. In magnonics or magnon spintronics, spin waves (or magnons) instead of electrical charge are utilized as carriers of information, circumventing energy waste from Joule heating induced by charge transport[1-10]. Compared to an electromagnetic wave at the same frequency range, the wavelengths of a spin wave (SW) are several orders of magnitude shorter, enabling magnonic devices at the nanometer scale[1,11]. In the past few years, various magnonic devices have been proposed, such as, spin-wave directional coupler[12-13], magnon transistor[14] and majority gate[15]. A major challenge in magnonic applications is to effectively control the transmission paths of a spin wave. Efficient channeling and steering of spin waves are crucial in the route towards programmable magnonic devices.

2. Artificial spin ices (ASIs) are magnetic metamaterials comprised of dipolar coupled magnetic nanoislands placed in a certain geometrical arrangement[16]. They are natural analogs of magnonic crystals for manipulating spin waves[4,10,17-31]. ASIs were initially introduced as a macroscopic model system mimicking the atomic spin frustration in the rare earth pyrochlore[16]. The field has since matured into an exciting research area[-21] for exploration of novel physical phenomena, such as geometrical frustration[16, 32], magnetic monopoles[33-34] and Coulomb phases[35]. Its reconfigurable aspect has allowed unique functionalities for applications, such as data storage[18,21] and advanced computations[36-37]. Recent studies demonstrate that artificial spin ices possess rich mode spectra and tunable band structures in the GHz frequency range[17,26-30], which can be tailored by tuning the

geometry and the magnetization state of ASIs for desired functionalities. These results indicate that ASIs can have great potential for programmable magnonics.

3. Here, we design a writable magnonic device which consists of a chiral or pinwheel ASI on top of a soft ferromagnetic thin film [Fig. 1(a)]. Through micromagnetic simulations we demonstrate that nanocale channels of spin wave transmission can be produced in the thin film under zero bias magnetic field. These nanochannels are regulatable by tuning the magnetization configuration of the top pinwheel ASI. The reconfigurability and rewritability of the ASI[38-39] enables these nanochannels in the ferromagnetic film to be globally switchable and locally writable. Our conceptual demonstration of writable magnonics could pave a new way for designing programmable spin-wave-based logic devices and circuits.

4. Recently, ferromagnetic thin film was introduced as an underlayer for an ASI system to tune the latter's frustration[40] and spin wave modes[23]. Here, we demonstrate the possibility for realizing writable magnonics in an ASI-mediated magnetic film [Fig.1(a)], by taking advantage of the reconfigurability and rewritability of the ASI to create and control nano-scale spin wave paths in the underlayer. For our simulations, we chose the newly developed pinwheel ASI pattern, conceived by rotating each nanobar magnet in a square lattice by 45^{o} around its center[41-45] as illustrated in Fig.1(b). The pinwheel ASI manifests novel properties, such as emergent charility[41] and domain wall topology[43]. One of its unique features is the formation of reconfigurable parallel chains of magnetic charges[43,45], which has been used to design programmable superconducting electronic devices[45]. In our simulations, we use elliptical nanobar magnets with dimensions of length

L = 300 nm, width W = 80 nm and thickness T = 20 nm [Fig.1(b)] and the underlying ferromagnetic film [fig.1(a)] is 10 nm thick. The micromagnetic simulations were carried out with Mumax3[46]. The materials' parameters are those of permalloy[46-48] for both the nanomagnetic bars and the underlying ferromagnetic film: saturation magnetization M_S = 8.6×10^5 A/m; damping α = 0.01; and exchange constant A_{ex} = 13×10^{-12} J/m. The magnetocrystalline anisotropy is not considered. Details of the micromagnetic simulations are described in the supplementary material.

5. The pinwheel ASI has four-fold degenerate ferromagnetic orders, which are easily tunable by applying an in-plane external magnetic field[43,45]. The black arrows in Figs. 2(a) and 2(b) show two of its degenerate magnetic configurations. Since an ASI made of 20 nm thick nanomagnets is athermal, these ordered configurations are stable under zero bias magnetic field at room temperature. The corresponding magnetization distribution of the underlying ferromagnetic film for these two ordered ASI configurations, displays vertical [Fig. 2(a)] and horizontal [Fig. 2(b)] meandering stripes of domain and domain walls in the absence of an external field, respectively. The two states are obtained by polarizing the sample with horizontal (for vertical domain state) and vertical (for horizontal domain state) in-plane magnetic fields, respectively. Therefore, it is easy to switch between the two states by tuning the magnetic configuration of the ASI pinwheel pattern. Furthermore, due to the athermal nature of the ASI, the in-plane magnetic field can be removed once the nanomagnets are polarized, so that the device can work at zero bias magnetic field.

6. Previous investigations have shown that domain walls can serve as excellent magnonic waveguide channels for spin wave propagation[49]**.** This suggests that the reconfigurable

domains and/or domain walls in the underlying magnetic film mediated by the pinwheel ASI could be considered as a perfect magnonic crystal for in-situ control of spin wave transmissions. To examine the spin wave dynamics in our continuous magnetic film, we calculate the mode spectra for the vertical and horizontal domain states, as shown in Fig. 2(c). The excitation of the external magnetic field pulse is along $+x$ (horizontal) direction in the sample plane. The spectra are calculated for both the top pinwheel ASI pattern and the underlayer film with periodic boundary conditions in the x-y plane. Both spectra show prominent peaks (V_1 for vertical domain state and H_1 for horizontal domain state) of eigenmodes with amplitudes much larger than the other minor modes V_2, H_2 and H_3 [Fig. 2(c)]. However, the spectra of the vertical and horizontal domain states are quite distinct, i.e., in both their mode frequencies and amplitudes. The prominent eigenmodes of the horizontal/vertical domain states are at 3.71/4.30 GHz while the amplitude of the horizontal horizontal domain state is nearly three times higher than that of the vertical domain state.

7. To investigate the origin of the spectrum eigenmodes, we also calculate the spatial mode profiles of various frequencies in the horizontal/vertical domain states. The spectrum maps of the top ASI and the underlayer film (see Figs. S1 and S2 in the supplementary material) clearly show that these eigenmodes are dominated by the responses from the underlayer film. Therefore, in the following studies we will focus on the spin wave responses from the underlayer film. In Figs. 2(d) and 2(e), we show the spatial mode profiles at H_1 = 3.71 GHz in the underlayer film for the two domain states, respectively. The spatially resolved maps for the other modes can be found in Figs. S1 and S2 in the supplementary material. The vertical domain state displays discrete, weak and diffusive modes [Fig. 2(d)]. In contrast, the horizontal domain state shows continuous, strong and

clear nanochannels of the mode at the domain walls. This agrees well with the domain wall based magnonic waveguides[49]. The reason for the absence of strong mode channels at the domain walls for the vertical domain state is that the magnetic moments in the domain walls are all along the *x* (horizontal) direction [Fig. 2(a)], which is the same with the excitation orientation of the microwave pulse. On the other hand, the magnetic moments of the domain walls in the horizontal domain state are all in the vertical direction [Fig. 2(b)], which is perpendicular to the microwave pulse direction. Therefore, strong resonance of moment precession in the domain walls is produced. We also investigated the spin wave excitations along y and z directions (see Figs. S3 and S4 in the supplementary material). The significantly different responses between vertical and horizontal domain states are indicative of a perfect reconfigurable magnonic crystal, in which the spin wave transmission can be conveniently switched on and/or off by tuning the magnetic configurations of the top ASIs. The spectra with in-plane microwave excitations can be conveniently realized by broadband ferromagnetic resonance (FMR) experiments by patterning samples on top of a coplanar waveguide (CPW)[24-27,30] or mounting samples on a CPW chip with a flip-chip technique[29]. Thus, our findings could be directly realized in experiments.

8. To further demonstrate the reconfigurable propagation of spin waves, we simulate a larger area of the sample. We apply a continuous excitation field (a sinusoidal field at H_1= 3.71GHz along the *x* direction) in a 10 nm wide center line, as shown in Figs. 3(a) and 3(c). The detailed simulation protocol is described in the supplementary material. Video 1 and 2 show time-dependent magnetic moment mappings in the two magnetic states, respectively, directly revealing the spin wave propagations in each state. We extract the spatial maps of

the spin wave amplitude in the underlayer film, as displayed in Figs. 3(b) and 3(d). It shows that the transmission of spin wave is limited to a narrow range near the center excitation line and cannot propagate over a long distance in the horizontal direction [Video 1 and Fig. 3(b)]. This is consistent with the weak spin wave mode in the vertical domain state under an excitation in the *x* direction [Fig. 2(d)]. In contrast, in the horizontal domain state with strong mode channels [Fig. 2(e)], the spin wave transmits over a much longer distance along the horizontal nanochannels [Video 2 and Fig. 3(d)]. These results directly demonstrate in-situ switchable spin wave propagation by reconfiguring the magnetization states of the top layer pinwheel ASI structure.

9. Recent state-of-the-art nanomagnetic writing techniques allow local control of magnetic configurations of the ASI using the tip of a magnetic force microscope[38-39]. This approach can be used to realize writable spin wave nanochannels in our ASI mediated magnetic film. To demonstrate this concept, we simulate the spin wave propagation in a composite magnetization state, in which the left/right sides of the excitation line is in the vertical/horizontal domain states, respectively [Fig. 4(a)]. The magnetic configurations of the composite state are shown in Fig. S5(a) in the supplemental material. Such a state is nearly impossible to achieve with a global magnetization process, but can be conveniently realized by the above mentioned magnetic writing techniques[38-39]. The spatially resolved mode of H_1 = 3.71 GHz displays the expected feature, i.e., the mode nanochannels appear only on the right side [Fig. 4(c)], resulting in a one-way spin wave propagation, as clearly displayed by Video 3 and Fig. 4(e). The polarity of such a one-way spin wave propagation can be reversed by writing a vertical domain state in the right side and a horizontal domain state in the left side [Video 5 and Fig. S6]. Furthermore, we can also design a magnetization

state in which a narrow strip of horizontal domain state is embedded within a vertical domain environment [Fig. 4(b)]. In this case, the nanochannels of spectrum mode are limited to the narrow strip region [Fig. 4(d)], leading to spin waves propagating primarily along the horizontal strip [Video 4 and Fig. 4(f)]. These examples evidently demonstrate writable magnonics in our ASI mediated ferromagnetic film, by fully taking advantage of the global reconfiguration and local rewrite characteristic of the ASI[38-39] system.

10. In summary, we introduced a reconfigurable magnonic crystal comprised of a pinwheel ASI pattern imprinted onto a soft ferromagnetic underlayer film. Using micromagnetic simulations, we showed that vertical and/or horizontal meandering stripes of magnetic domains and domain walls in the underlayer film can be induced by tuning the magnetic configuration of the top pinwheel ASI structure. These magnetic domains and domain walls are stable at zero bias magnetic field. Furthermore, the domain walls can sustain spin waves with well-defined frequency, providing nanochannel waveguides that are switchable and writable. Our results demonstrate a convenient and flexible approach to effectively guide and manipulate spin waves, highlighting a new application of artificial spin ices for writable magnonics. This highly reconfigurable magnonic crystal would stimulate future magnonic applications, such as programmable spin wave circuits and logic devices for energy-efficient information and data processing.

ACKNOWLEDGMENTS

This work is supported by the National Key R&D Program of China (2018YFA0209002), the National Natural Science Foundation of China (61771235, 12074189, 61971464, 61727805 and 11961141002), Jiangsu Excellent Young Scholar program (BK20200008) and Jiangsu Shuangchuang program. Part of the project design (Z.L.X.) and manuscript writing (Z.L.X. and W.K.K.) are supported by the U.S. Department of Energy, Office of Science, Basic Energy Sciences, Materials Sciences and Engineering. Z.L.X. also acknowledges support from the National Science Foundation under Grant No. DMR-1901843 for his efforts on data analysis Y.D. acknowledges support from the Major Scientific Research Project of Zhejiang Lab (2019MB0AD01).

DATA AVAILABILITY

The data that support the findings of this study are available from the corresponding author upon reasonable request.

REFERENCES：

[1] S. Neusser and D. Grundler, Magnonics: spin waves on the nanoscale, Adv. Mater. **21**, 2927 (2009).

[2] V.V. Kruglyak, S.O. Demokritov, D. Grundler, Magnonics, J. Phys. D: Appl. Phys. **43**, 264001 (2010).

[3] B. Lenk, H. Ulrichs, F. Garbs, M. Münzenberg, The building blocks of magnonics, Phys. Rep. **507**, 107 (2011).

[4] A. Barman, G. Gubbiotti, S. Ladak et al., The 2021 magnetism roadmap, J. Phys. Condens. Matter Phys. **33**, 413001 (2021).

[5] A.V. Chumak, V.I. Vasyuchka, A.A. Serga, B. Hillebrands, Magnon spintronics, Nat. Phys. **11**, 453 (2015).

[6] A. Chumak, A. Serga, B. Hillebrands, Magnonic crystals for data processing, J. Phys. D: Appl. Phys. **50**,244001 (2017).

[7] G. Csaba, Á. Papp, W. Porod, Perspectives of using spin waves for computing and signal processing, Phys. Lett. A **381**,1471 (2017).

[8] H. Yu, J. Xiao, and H. Schultheiss, Magnetic texture based magnonics, Phys. Rep. **905**, 1 (2021).

[9] A. Mahmoud, F. Ciubotaru, F. Vanderveken, A. V. Chumak, S. Hamdioui, C. Adelmann, and S. Cotofana, Introduction to Spin Wave Computing, J. Appl. Phys. **128**, 161101 (2020).

[10] M. Krawczyk and D. Grundler, Review and prospects of magnonic crystals and devices with reprogrammable band structure, J. Phys.: Condens. Matter **26**, 123202 (2014).

[11] E. Albisetti, D. Petti, G. Sala, R. Silvani, S. Tacchi, S. Finizio, S. Wintz, A. Calò, X. Zheng, J. Raabe et al., Nanoscale Spin-Wave Circuits Based on Engineered Reconfigurable Spin-Texture, Commun. Phys. **1**, 56 (2018).

[12] Q. Wang, P. Pirro, R. Verba, A. Slavin, B. Hillebrand, and A. V. Chunmak, Reconfigurable nanoscale spin-wave directional coupler, Sci.Adv. **4**, e1701517 (2018).

[13] Q. Wang, M. Kewenig, M. Schneider, R. Verba, F. Kohl, B. Heinz, M. Geilen, M. Mohseni, B. Lägel, F. Ciubotaru, C. Adelmann, C. Dubs, S. D. Cotofana, O. V. Dobrovolskiy, T. Brächer, P. Pirro and A. V. Chumak, A magnonic directional coupler for integrated magnonic half-adders, Nat. Electron. **3**, 765 (2020).

[14] A. V. Chumak, A. A. Serga, and B. Hillebrands, Magnon transistor for all-magnon data processing, Nat. Commun. **5**, 4700 (2014).

[15] G. Talmelli, T. Devolder, N. Träger, J. Förster, S. Wintz, M. Weigand, H. Stoll, M. Heyns, G. Schutz, I. P. Radu, J. Gräfe, F. Ciubotaru, and C. Adelmann, Reconfigurable submicrometer spin-wave majority gate with electrical transducers, Sci. Adv. **6**, eabb4042 (2020).

[16] R. F. Wang, C. Nisoli, R. S. Freitas, J. Li, W. McConville, B. J. Cooley, M. S. Lund, N. Samarth, C. Leighton, V. H. Crespi, and P. Schiffer,Artificial ‘spin ice’ in a geometrically frustrated lattice of nanoscale ferromagnetic islands, Nature **439**, 303 (2006).

[17] S. Gliga, E. Iacocca, and O. G. Heinonen, Heinonen.Dynamics of reconfigurable artificial spin ice: Toward magnonic functional materials, APL Mater. **8**, 040911 (2020).

[18] C. Nisoli, R. Moessner, and P. Schiffer, Colloquium: Artificial spin ice: Designing and imaging magnetic frustration, Rev. Mod. Phys. **85**, 1473 (2013).

[19] I. Gilbert, C. Nisoli, and P. Schiffer, Frustration by design, Phys. Today **69**, 54 (2016).

[20] L. J. Heyderman and R. L. Stamps, Artificial ferroic systems: novel functionality from structure, interactions and dynamics, J. Phys.: Condens. Matter **25**, 363201 (2013).

[21] S. H. Skjærvø, C. H. Marrows, R. L. Stamps, and L. J. Heyderman, Advances in artificial spin ice, Nature Rev. Phys. **2**, 13 (2019).

[22] S. Gliga, A. Kákay, R. Hertel, and O. G. Heinonen, Spectral Analysis of Topological Defects in an Artificial Spin-Ice Lattice, Phys. Rev. Lett. **110**, 117205 (2013).

[23] E. Iacocca, S. Gliga, and O. Heinonen, Tailoring Spin-Wave Channels in a Reconfigurable Artificial Spin Ice, Phys. Rev. Appl. **13**, 044047 (2020).

[24] M. B. Jungfleisch, W. Zhang, E. Iacocca, J. Sklenar, J. Ding, W. Jiang, S. Zhang, J. E. Pearson, V. Novosad, J. B. Ketterson, O. Heinonen, and A. Hoffmann, Dynamic Response of an Artificial Square Spin Ice, Phys. Rev. B **93**, 100401(R) (2016).

[25] T. Dion, D. M. Arroo, K. Yamanoi, T. Kimura, J. C. Gartside, L. F. Cohen, H. Kurebayashi, and W. R. Branford, Tunable Magnetization Dynamics in Artificial Spin Ice via Shape Anisotropy Modification, Phys. Rev. B **100**, 054433 (2019).

[26] W. Bang, J. Sturm, R. Silvani, M. T. Kaffash, A. Hoffmann, J. B. Ketterson, F. Montoncello, and M. B. Jungfleisch, Influence of the Vertex Region on Spin Dynamics in Artificial Kagome Spin Ice, Phys. Rev. Appl. **14**, 014079 (2020).

[27] S. Lendinez and M. B. Jungfleisch, Magnetization dynamics in artificial spin ice, J. Phys.: Condens. Matter **32**, 013001 (2020).

[28] D. M. Arroo, J. C. Gartside, and W. R. Branford, Sculpting the spin-wave response of artificial spin ice via microstate selection, Phys. Rev. B **100**, 214425 (2019).

[29] J. C. Gartside, A. Vanstone, T. Dion, K. D. Stenning, D. M. Arroo, H. Kurebayashi, and W. R. Branford, Reconfigurable magnonic mode-hybridisation and spectral control in a bicomponent artificial spin ice, Nat. Commun. **12**, 2488 (2021).

[30] S. Lendinez, M. T. Kaffash, and M. B. Jungfleisch, Emergent spin dynamics enabled by lattice interactions in a bicomponent artificial spin ice, Nano Lett. **21**, 1921 (2021).

[31] E. Iacocca, S. Gliga, R. L. Stamps, and O. Heinonen, Reconfigurable wave band structure of an artificial square ice, Phys. Rev. B **93**, 134420 (2016).

[32] I. Gilbert, Y. Lao, I. Carrasquillo, L. O'brien, J. D. Watts, M. Manno, C. Leighton, A. Scholl, C. Nisoli, and P. Schiffer, Emergent Reduced Dimensionality by Vertex Frustration in Artificial Spin Ice, Nat. Phys. **12**, 162 (2016).

[33] E. Mengotti, L. J. Heyderman, A. F. Rodríguez, F. Nolting, R. V. Hügli, and H.-B. Braun, Real-space observation of emergent magnetic monopoles and associated Dirac strings in artificial kagome spin ice, Nat. Phys. **7**, 68 (2011).

[34] A. Farhan, M. Saccone, C. F. Petersen, S. Dhuey, R. V. Chopdekar, Y. L. Huang, N. Kent, Z. Chen, M. J. Alava, T. Lippert, A. Scholl, and S. van Dijken, Emergent Magnetic Monopole Dynamics in Macroscopically Degenerate Artificial Spin Ice, Sci. Adv. **5**, eaav6380 (2019).

[35] Y. Perrin, B. Canals, and N. Rougemaille, Extensive degeneracy, Coulomb phase and magnetic monopoles in artificial square ice, Nature **540**, 410 (2016).

[36] H. Arava, N. Leo, D. Schildknecht, J. Cui, J. Vijayakumar, P. M. Derlet, A. Kleibert, and L. J. Heyderman, Engineering Relaxation Pathways in Building Blocks of Artificial Spin Ice for Computation, Phys. Rev. Appl. **11**, 054086 (2019).

[37] F. Caravelli and C. Nisoli, Logical Gates Embedding in Artificial Spin Ice, New J. Phys. **22**, 103052 (2020).

[38] Y.-L. Wang, Z.-L. Xiao, A. Snezhko, J. Xu, L. E. Ocola, R. Divan, J. E. Pearson, G. W. Crabtree and W.-K. Kwok, Rewritable Artificial Magnetic Charge Ice, Science **352**, 962 (2016).

[39] J. C. Gartside, D. M. Arroo, D. M. Burn, V. L. Bemmer, A. Moskalenko, L. F. Cohen, and W. R. Branford, Realization of ground state in artificial kagome spin ice via topological defect-driven magnetic writing, Nat. Nanotechnol. **13,** 53 (2018).

[40] S. Kempinger, Y. S. Huang, P. Lammert, M. Vogel, A. Hoffmann, V. H. Crespi, P. Schiffer, and N. Samarth, Field-Tunable Interactions and Frustration in Underlayer-Mediated Artificial Spin Ice, Phys. Rev. Lett. **127**, 117203 (2021).

[41] S. Gliga, G. Hrkac, C. Donnelly, J. Büchi, A. Kleibert, J. Cui, A. Farhan, E. Kirk, R. V. Chopdekar, Y. Masaki, N. S. Bingham, A. Scholl, R. L. Stamps, and L. J. Heyderman, Emergent Dynamic Chirality in a Thermally Driven Artificial Spin Ratchet, Nat. Mater.**16**, 1106 (2017).

[42] R. Macêdo, G. M. Macauley, F. S. Nascimento, and R. L. Stamps, Apparent ferromagnetism in the Pinwheel Artificial Spin Ice, Phys. Rev. B **98**, 014437 (2018).

[43] Y. Li, G. W. Paterson, G. M. Macauley, F. S. Nascimento, C. Ferguson, S. A. Morley, M. C. Rosamond, E. H. Linfield, D. A. MacLaren, R. Ma^eedo, C. H. Marrows, S. McVitie, and R. L. Stamps, Superferromagnetism and Domain-Wall Topologies in Artificial "Pinwheel" Spin Ice, ACS Nano **13**, 2213 (2019).

[44] G. M. Macauley, G. W. Paterson, Y. Li, R. Macêdo, S. McVitie, and R. L. Stamps, Tuning magnetic order with geometry: Thermalization and defects in two-dimensional artificial spin ices, Phys. Rev. B **101**, 144403 (2020).

[45] Y.-Y. Lyu, X. Ma, J. Xu, Y.-L. Wang, Z.-L. Xiao, S. Dong, B. Janko, H. Wang, R. Divan, J. E. Pearson, P. Wu, and W.-K. Kwok, Reconfigurable Pinwheel Artificial-Spin-Ice and Superconductor Hybrid Device, Nano Lett. **20**, 8933 (2020).

[46] A.Vansteenkiste, J. Leliaert, M. Dvornik, M. Helsen, F. Garcia-Sanchez, and B.Van Waeyenberge, The design and verification of MuMax3, AIP Adv. **4**, 107133 (2014).

[47] K. S. Lee, D. S. Han, and S. K. Kim, Physical Origin and Generic Control of Magnonic Band Gaps of Dipole-Exchange Spin Waves in Width-Modulated Nanostrip Waveguides, Phys. Rev. Lett. **102**, 127202 (2009).

[48] K. D. Stenning, J. C. Gartside, T. Dion, A. Vanstone, D. M. Arroo, and W. R. Branford, Magnonic bending, phase shifting and interferometry in a 2D reconfigurable nanodisk crystal, ACS Nano **15**, 674 (2021).

[49] F. Garcia-Sanchez, P. Borys, R. Soucaille, J. P. Adam, R. L. Stamps, and J. V. Kim, Narrow magnonic waveguides based on domain walls, Phys. Rev. Lett. **114**, 247206 (2015).

Figures

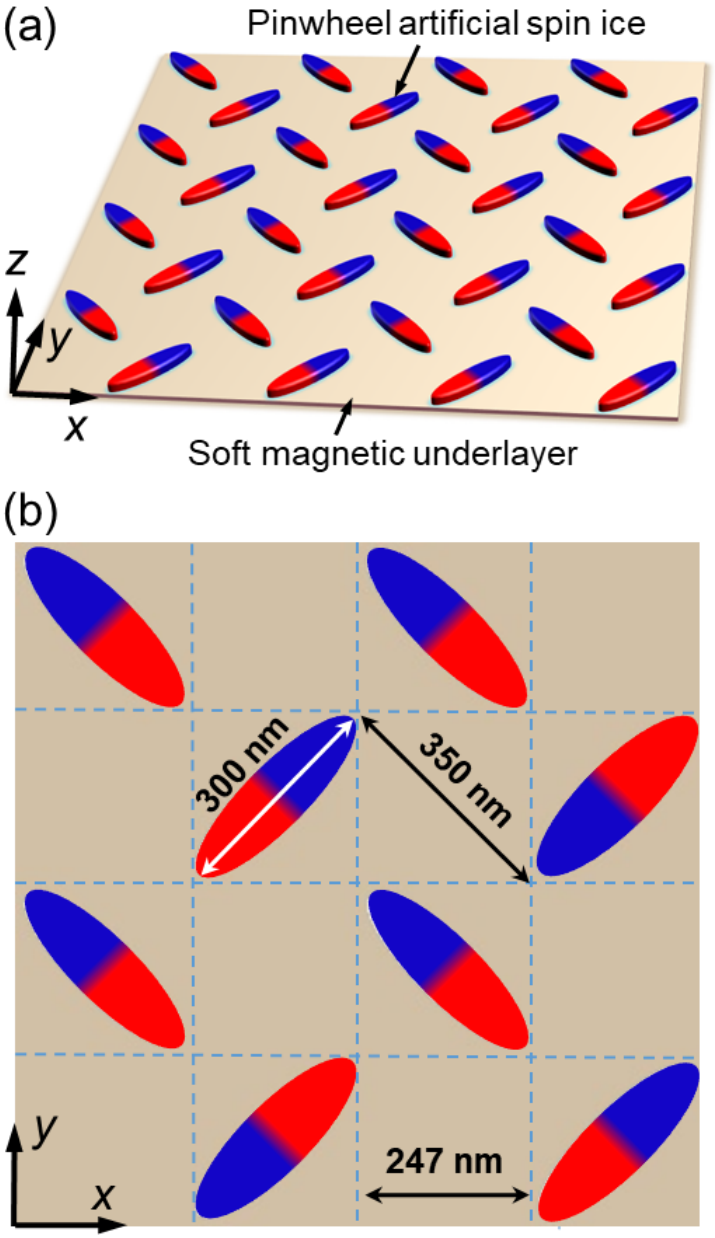

Fig. 1 | Design of a system with writable spin wave nanochannels. (a) Schematic showing a pinwheel artificial spin ice on top of an underlayer film. (b) Parameters of the top pinwheel artificial spin ice.

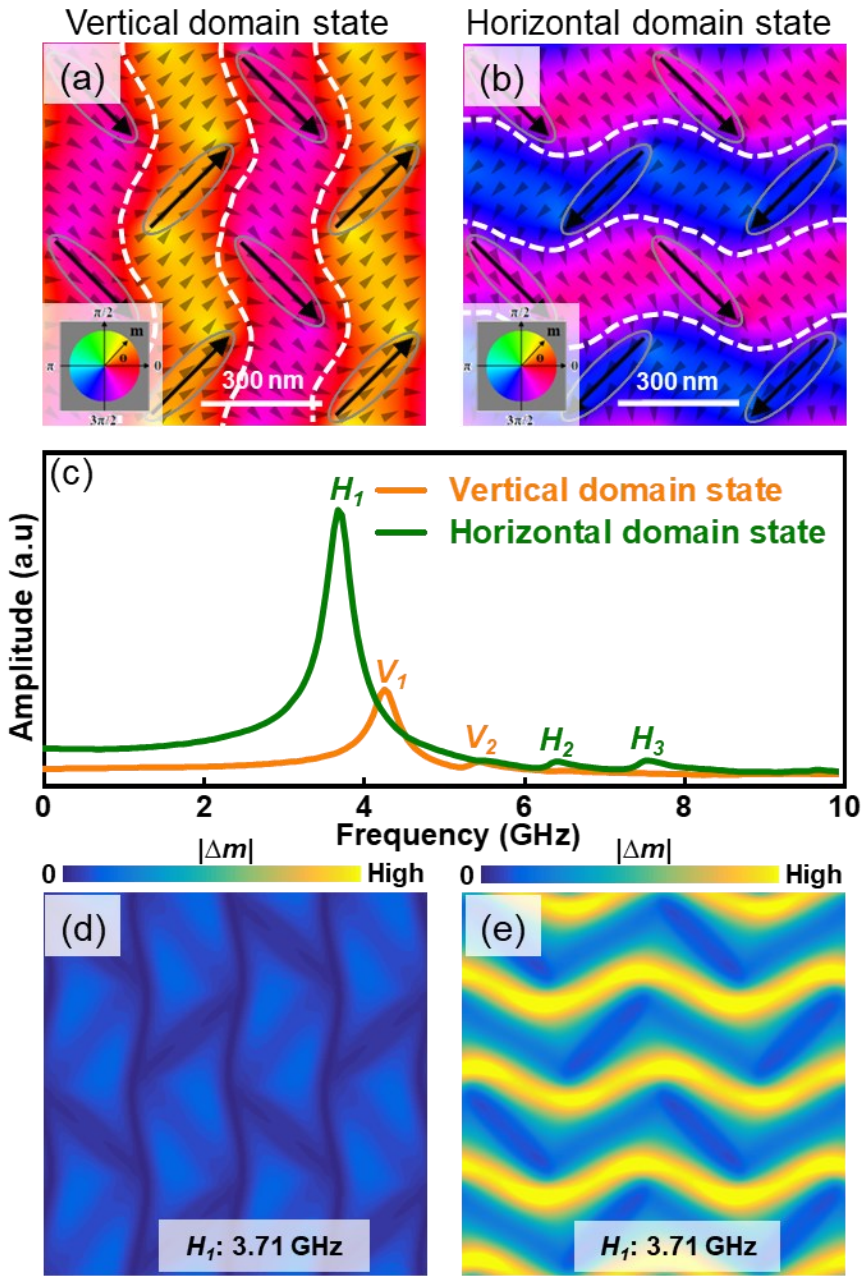

Fig. 2 | Tunable magnetic structures and spin wave spectra. (a) and **(b)** Vertical and horizontal stripe domains and domain walls in the soft magnetic underlayer film at zero external magnetic field, respectively. The black arrows show the corresponding magnetic configurations of the top pinwheel ASI structure. The white dash lines are domain walls. **(c)** The spectra for vertical and horizontal stripe states excited by a field pulse along the x (horizontal) direction [defined in Fig. 1(b)]. The mode frequencies are H_1 = 3.71 GHz, H_2 = 6.50 GHz, H_3= 7.62 GHz, V_1 = 4.30 GHz, V_2 = 5.47 GHz. **(d)** and **(e)** Spatially resolved modes at H_1 = 3.71 GHz for the vertical and horizontal stripe states, respectively.

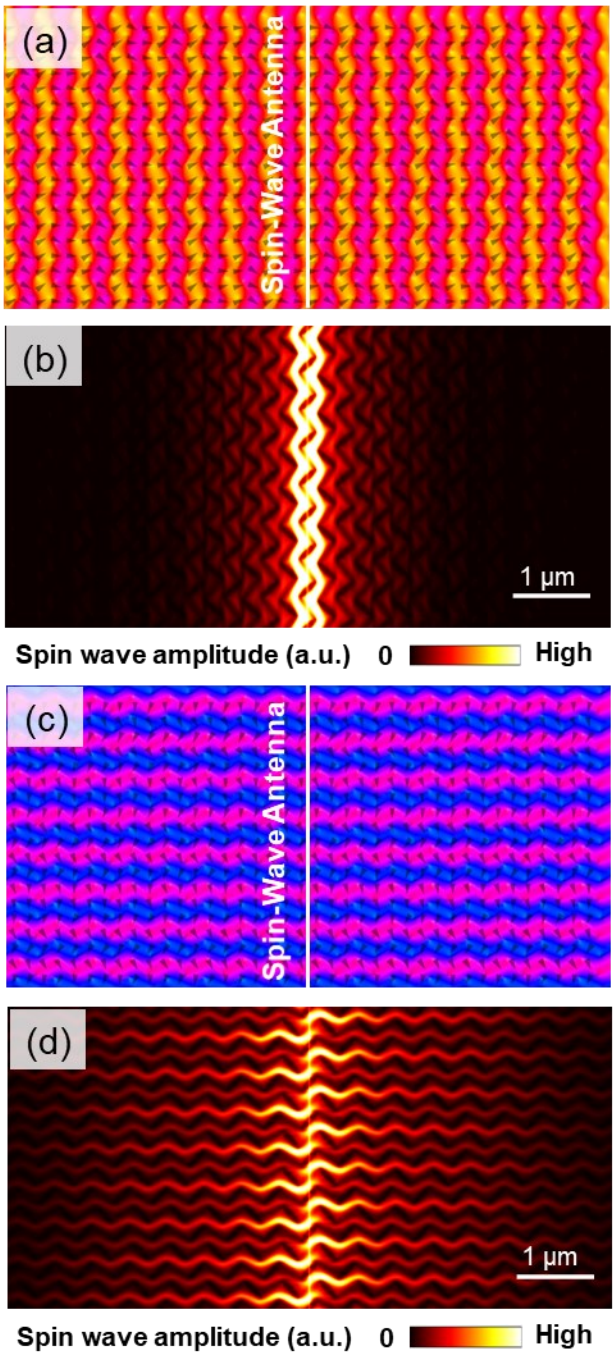

Fig. 3 | Switchable spin wave propagation. (a) and **(b)** Micromagnetic configuration and spin wave amplitude map of the vertical domain state, respectively, with the spin wave excitation in the white center line. **(c)** and **(d)** Micromagnetic configuration and spin wave amplitude map of the horizontal domain state, respectively.

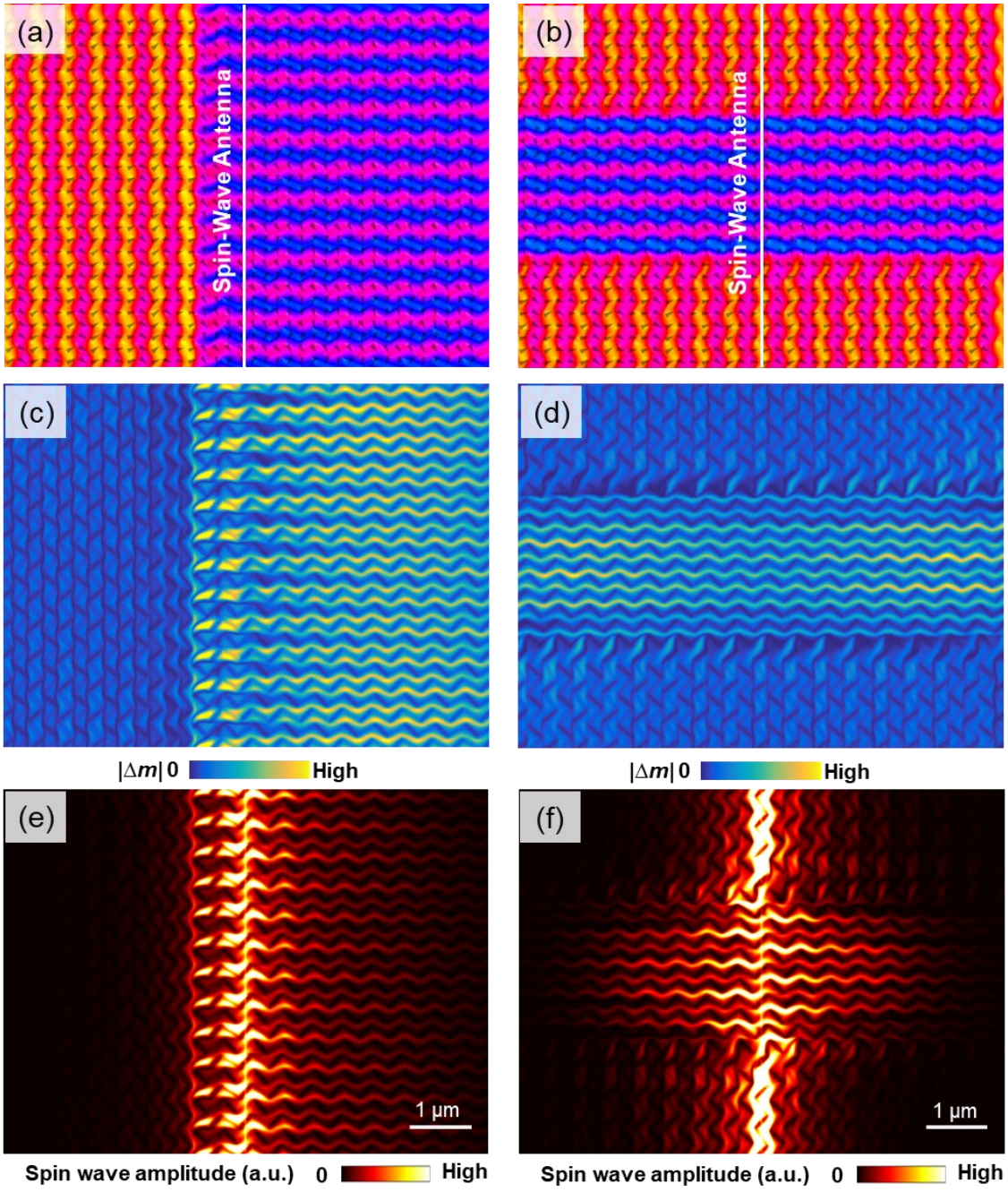

Fig. 4 | Writable spin wave nanochannels. (a) and **(b)** Composite magnetization state with both vertical and horizontal domain states, which can be realized by tuning the magnetization configurations of the ASI via currently available magnetic writing techniques (see main text). **(c)** and **(d)** Spatially resolved modes at H_1 = 3.71 GHz corresponding to (a) and (b). **(e)** and **(f)** Amplitude maps of propagating spin waves, corresponding to the states in (a) and (b), respectively. The spin waves are excited from the white center line shown in (a) and (b).

Supplementary material

Simulations of the magnetization states and the spin wave spectra. The simulations are initialized with prescribed magnetization states for the pinwheel patterned ASI nanomagnets and with a uniform state for the underlayer ferromagnetic film. To eliminate relaxation ringing effects at low damping, the entire system relaxes to the ground state at zero magnetic field using a combination of high damping $\alpha = 1$ for 10 ns and a realistic damping of $\alpha = 0.01$ for 20 ns[34]. The simulations in Fig. 2 are conducted under a periodic boundary condition in the *x*-*y* plane. The cell size is 1.93nm × 1.93nm × 5nm. The system is excited by applying a uniform magnetic field pulse B_{ext} = 2 mT for 50 ps along various directions described in the main text. We record the time dependent magnetization $\boldsymbol{m}(x, y, z, t)$ of all cells every 10 ps over the subsequent 20 ns. The fluctuations of $\boldsymbol{m}(x, y, z, t)$ are calculated for all cells via $\Delta m(x,y,z,t) = m(x,y,z,t) - m(x,y,z,t_0)$, where $\boldsymbol{m}(x,y,z,t_0)$ corresponds to the ground state. The spectra are obtained from Fourier transformation of spatially averaged $\Delta m(x,y,z,t)$. The spin wave mode profile for a specific frequency can be mapped out as a function of position, $|\Delta m| = \sqrt{(\Delta m_x)^2 + (\Delta m_y)^2 + (\Delta m_z)^2}$.

Simulations of spin wave transmission. A larger sample of 10.15 μm × 10.15 μm is used for simulating the propagation of spin waves with open boundary conditions. The used cell size is 10 nm × 10 nm × 10 nm. In order to avoid boundary effect, we collect the data at the center region of the sample. A sinusoidal field $B_x = Asin(2\pi ft)$ with frequency f = 3.71 GHz and amplitude A = 2 mT is locally applied to the 10 nm wide center region along the *x* direction. We record the magnetization $m(x, y, z, t)$ every 10 ps. The fluctuations

$m(x,y,z,t)$ were calculated for all cells via $\Delta m(x,y,z,t) = m(x,y,z,t) - m(x,y,z,t_0)$, where $m(x,y,z,t_0)$ corresponds to the ground state. The spin wave spatial amplitude map is calculated via

$$\left|\mathrm{A}(t)\right| = \sqrt{(\Delta m(x,t)_{\max})^2 + (\Delta m(y,t)_{\max})^2 + (\Delta m(z,t)_{\max})^2} \ .$$

For the spin wave propagations shown in videos 1-5, the fluctuations $m(x,t)$ are calculated for all cells via $\Delta m(x,t) = m(x,t) - m(x,t_0)$, where $m(x,t_0)$ corresponds to the ground state. The spatial propagation of the spin wave is mapped out as a function of both $\Delta m(x,t)$ and position.

Spin wave spectra with *y*- and *z*-direction excitations. The spin wave excitations are not only determined by the magnetic configurations of the sample system, but also significantly influenced by the direction of the driving microwaves. We also simulate the spin wave spectra driven by microwave pulses along *y* and *z* directions. The results can be found in Figs. S3 and S4, respectively. The spectrum responses of both frequency [Figs. S3(a)] and spatial dependence [Figs. S3(b) and S3(c)] for the two domain states excited with a *y*-direction microwave pulse are simply reversed from the *x*-direction microwave pulse [Figs. 2(c)-2(e)]. In this case, the vertical domain state shows clear nanochannels of magnonic mode, which are not observed in the horizontal domain state. The reversal in *y*-direction microwave excitations can be easily understood by analyzing the orientation of the moments in domain walls and that of the driving microwave pulse, the same analysis used for *x*-direction excitations. For the case of out-of-plane microwave excitation along the *z*-direction, which is perpendicular to the domain wall moments (in-plane) for both states, the spectra are exactly identical for both vertical and horizontal domain states, as shown in

Fig. S4(a). The prominent modes for both states display continuous nanochannels (but with orthogonal directions for both states) under *z* direction microwave excitation [Fig. S4(b) and S4(c)]. However, the mode is much weaker than those from the in-plane microwave excitations.

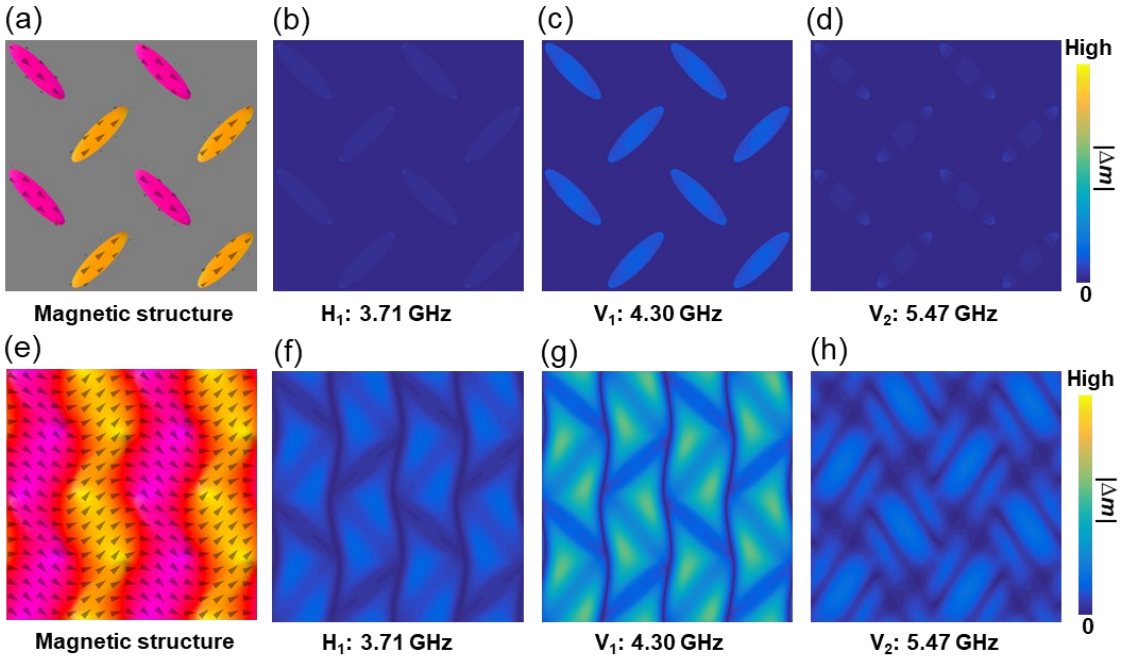

Fig. S1 | Spatially resolved modes for vertical domain state. (a) Micromagnetic structure of the top pinwheel ASI in the ground state. (b)-(d) Spatially resolved modes of H_1, V_1, V_2 [defined in Fig. 2(c)] for the top pinwheel ASI, respectively. **(e)** Micromagnetic structure of the underlayer film in the ground state. (f)-(h) Spatially resolved modes of H_1, V_1, V_2 in the underlayer film. The color scales of the mode maps are identical. The mode amplitudes of the underlayer are much stronger than those of the top ASI structure, suggesting that these eigenmodes are dominated by the responses from the underlayer film.

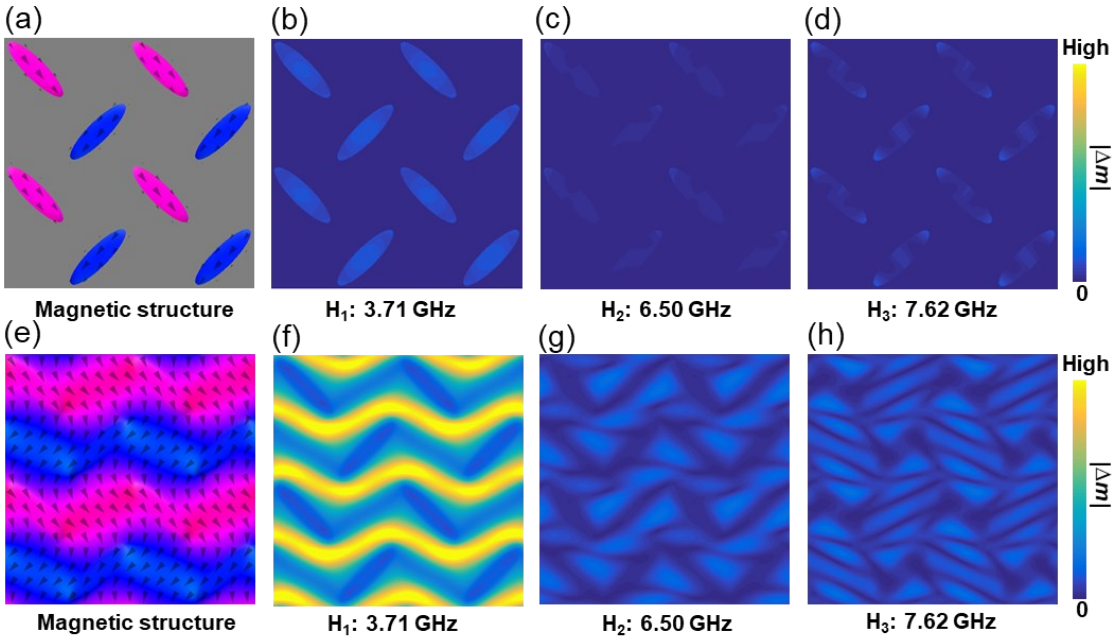

Fig. S2 | Spatially resolved modes for horizontal stripe state. (a) Micromagnetic structure of the top pinwheel ASI in the ground state. (b)-(d) Spatially resolved modes of H_1-H_3 [defined in Fig. 2(c)] for the top pinwheel ASI. **(e)** Micromagnetic structure of the underlayer film in the ground state. (f)-(h) Spatially resolved modes of H_1-H_3 in the underlayer film. The color scales of the mode maps are identical. The mode amplitudes of the underlayer film are much stronger than those of the top ASI, suggesting that these eigenmodes are dominated by the responses from the underlayer film.

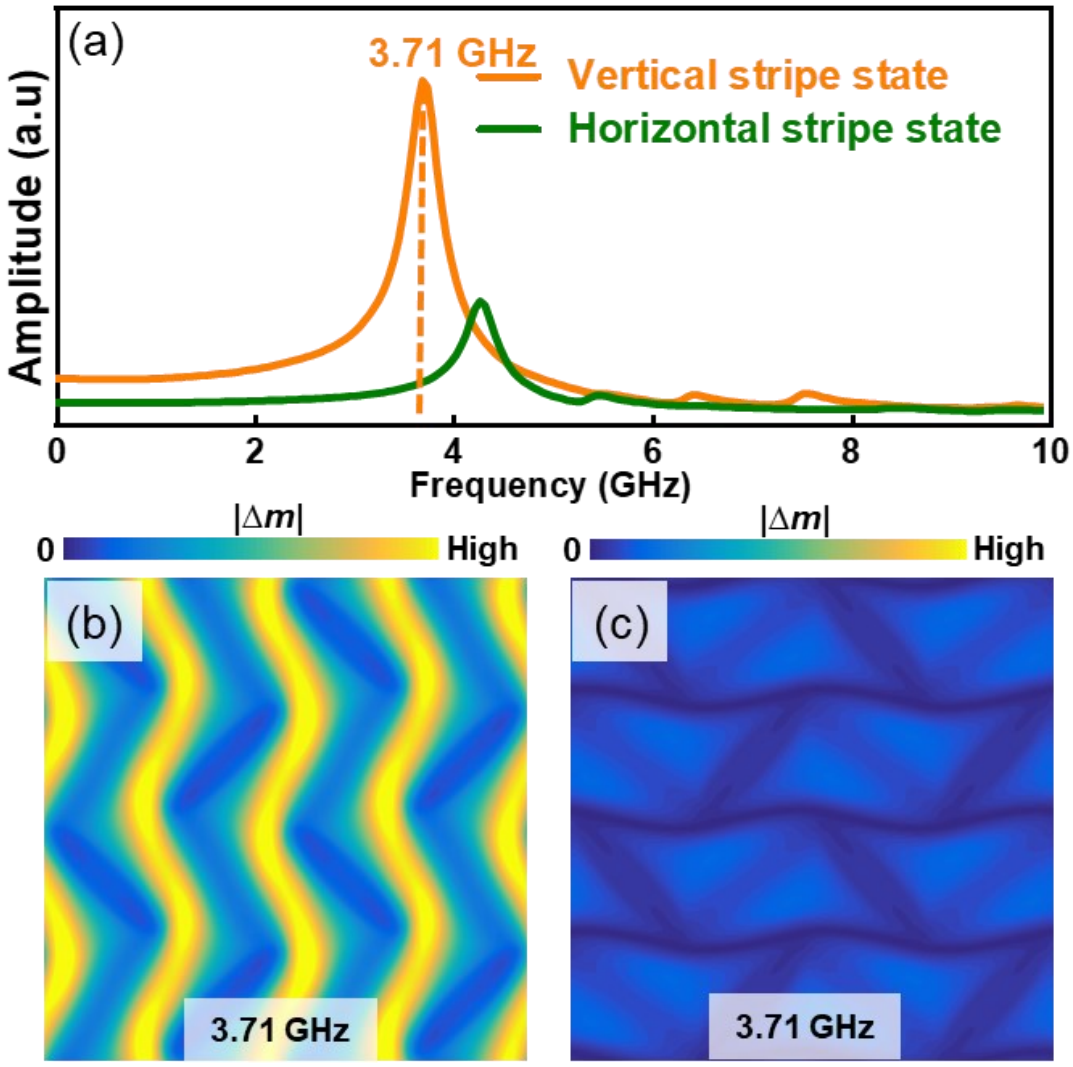

Fig. S3 | Spin wave spectra with y-direction excitation. (a) Spectra for vertical and horizontal domain states excited by a field pulse along *y* direction (defined in Fig. 1a). The axis scale is the same as that in Fig. 2(c). **(b)** and **(c)** Spatially resolved modes at 3.71 GHz corresponding to the two spectra in (a) and for the vertical and horizontal domain states, respectively. The color scale is the same as that in Figs. 2(d) and 2 (e).

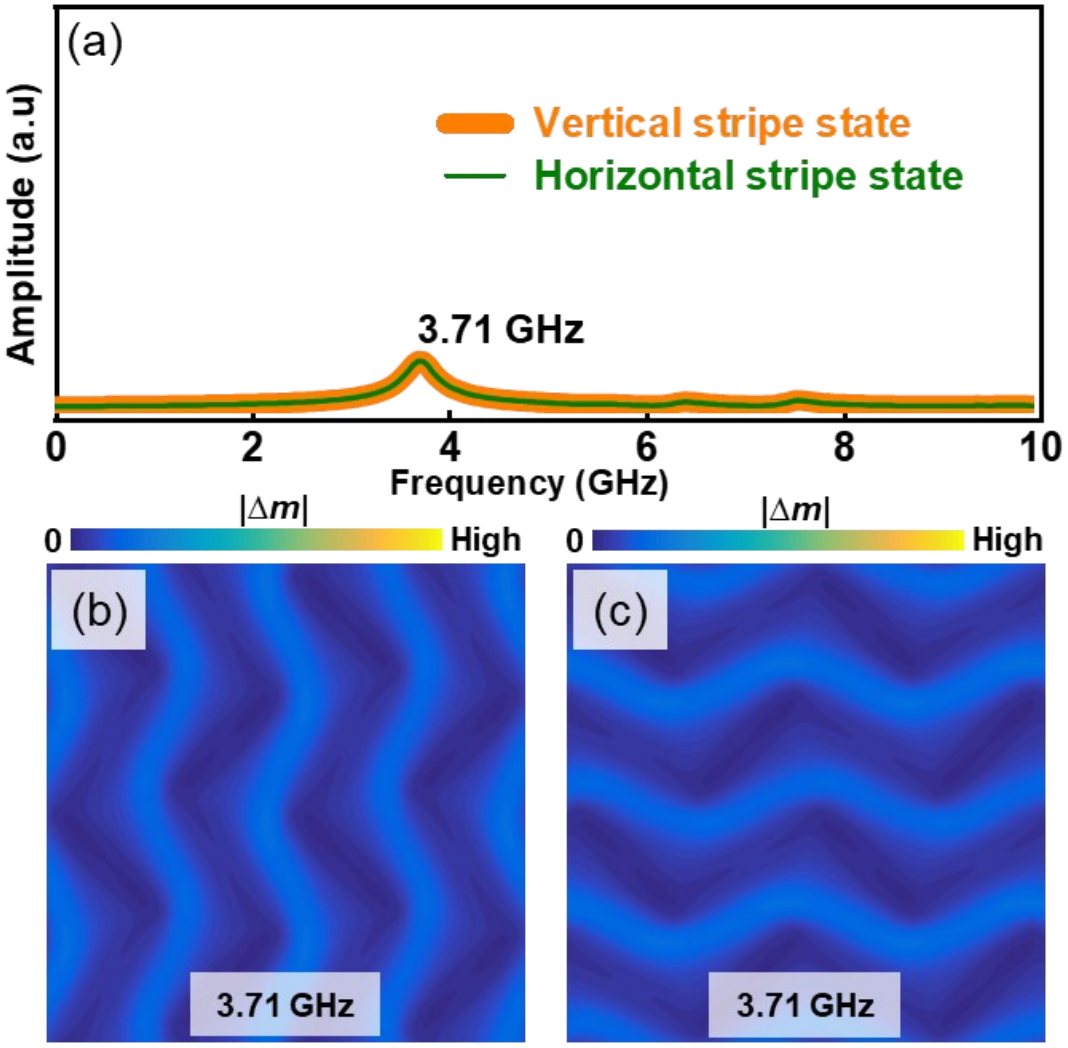

Fig. S4 | Spin wave spectra with z-direction excitation. (a) The spectra for vertical and horizontal domain states excited by a field pulse along the *z* direction (defined in Fig. 1a). The axis scale is the same as that in Fig. 2(c). **(b)** and **(c)** Spatially resolved modes at 3.71 GHz corresponding to the two spectra in (a) and for the vertical and horizontal domain states, respectively. The color scale is the same as that in Figs. 2(d) and 2 (e).

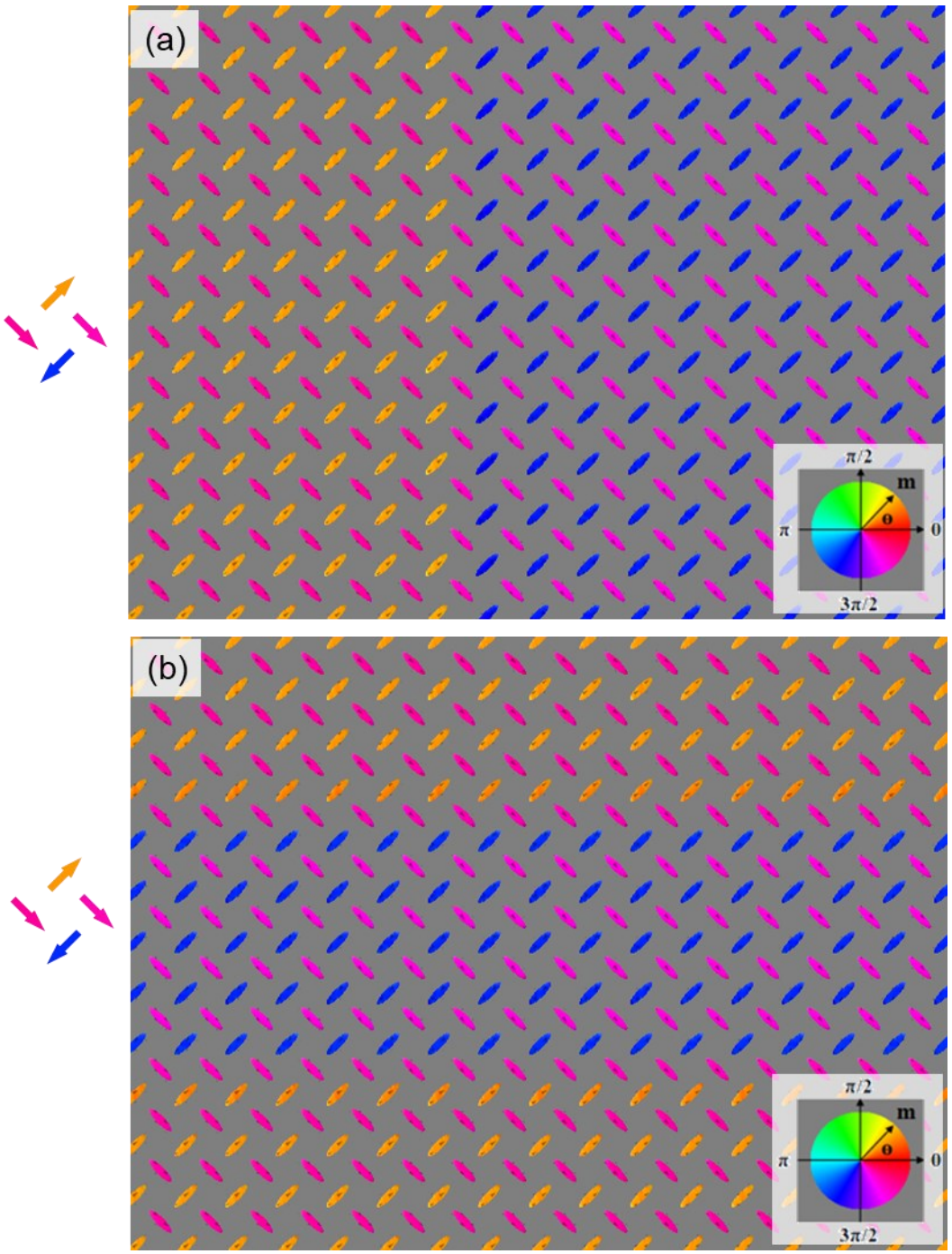

Fig. S5 | Magnetic configurations of the top pinwheel ASI in the composite states. (a) and **(b)** correspond to Fig. 4(a) and 4(b), respectively. The color encoded moment directions of the nanomagnets are shown by the arrows in the left.

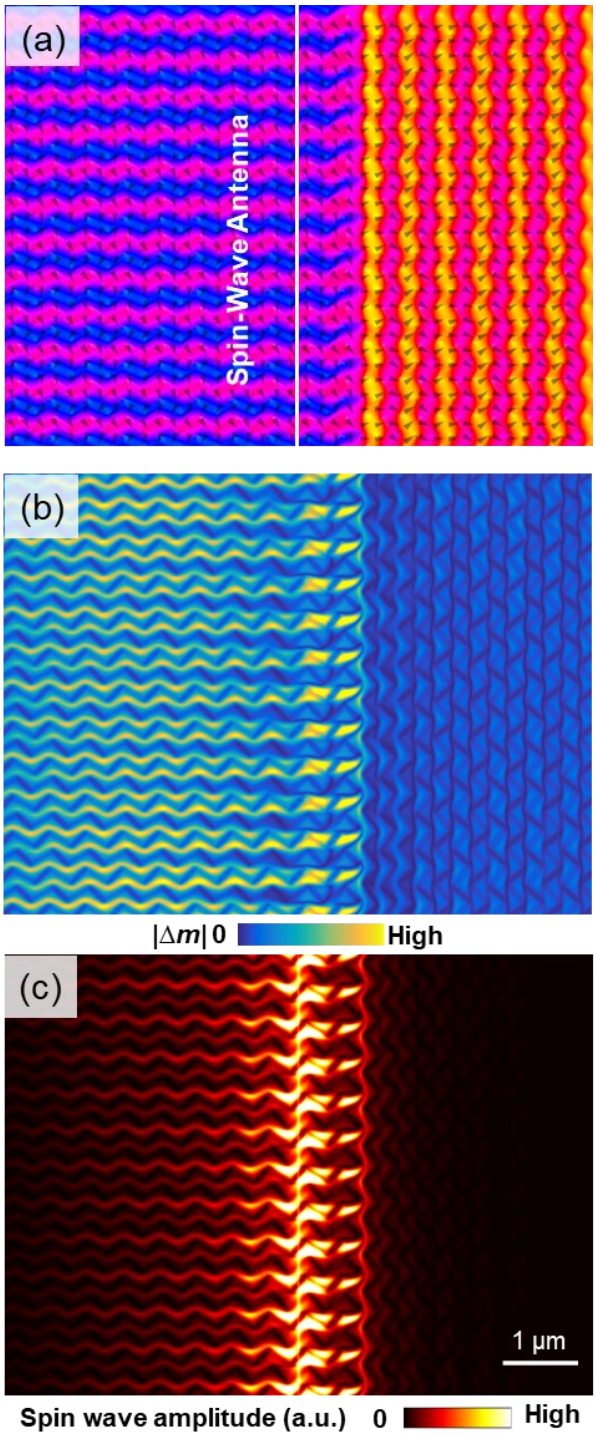

Fig. S6 | Reversible one-way spin wave propagation. (a) Composite magnetization state with a vertical domain state on the right of a horizontal domain state, which is opposite to that in Fig. 4(c). **(b)** and **(c)** Associated spatially resolved modes at H_I = 3.71 GHz and spin wave amplitude map of propagating spin waves. The spin waves are excited from the white center line shown in (a). Scale bar, 1 μm.

Video 1. Spin wave propagation in the vertical domain state in Fig. 3(a).

Video 2. Spin wave propagation in the horizontal domain state in Fig. 3(c).

Video 3. Spin wave propagation in the composite state in Fig. 4(a).

Video 4. Spin wave propagation in the composite state in Fig. 4(b).

Video 5. Spin wave propagation in the composite state in Fig. S6(a).